ADVANCED HEALTHCARE MATERIALS

Supporting Information

for *Adv. Healthcare Mater.*, DOI 10.1002/adhm.202203028

Endogenous/Exogenous Nanovaccines Synergistically Enhance Dendritic Cell-Mediated Tumor Immunotherapy

Yu Zhang, Qiang Li, Meng Ding, Weijun Xiu, Jingyang Shan, Lihui Yuwen, Dongliang Yang, Xuejiao Song, Guangwen Yang, Xiaodan Su, Yongbin Mou, Zhaogang Teng* and Heng Dong**

Supporting Information

Endogenous/Exogenous Nanovaccines Synergistically Enhance Dendritic Cell-mediated Tumor Immunotherapy

Yu Zhang[#], Qiang Li[#], Meng Ding, Weijun Xiu, Jingyang Shan, Lihui Yuwen, Dongliang Yang, Xuejiao Song, Guangwen Yang, Xiaodan Su, Yongbin Mou,[*] Zhaogang Teng,[*] and Heng Dong[*].

Y.Z., Q.L., M.D., G.Y., Prof. Y.M., H.D.

Nanjing Stomatological Hospital, Medical School of Nanjing University

30 Zhongyang Road, Nanjing, 210008 Jiangsu, P.R. China

E-mail: Y.M. yongbinmou@nju.edu.cn; H.D. dongheng90@smail.nju.edu.cn

X.W., Prof. L.Y., Prof. X.S., Prof. Z.T.

Key Laboratory for Organic Electronics and Information Displays

Jiangsu Key Laboratory for Biosensors, Institute of Advanced Materials

Jiangsu National Synergetic Innovation Centre for Advanced Materials

Nanjing University of Posts and Telecommunications

9 Wenyuan Road, Nanjing, 210023 Jiangsu, P.R. China

E-mail: Z.T. iamzgteng@njupt.edu.cn

J.S.

Department of Neurology, Shenzhen Institute of Translational Medicine, The First Affiliated Hospital of Shenzhen University,

Shenzhen Second People's Hospital, Shenzhen 518000, China

Prof. D. Y., Prof. X. S

School of Physical and Mathematical Sciences, Nanjing Tech University,

30 South Puzhu Road, 211816 Nanjing, China

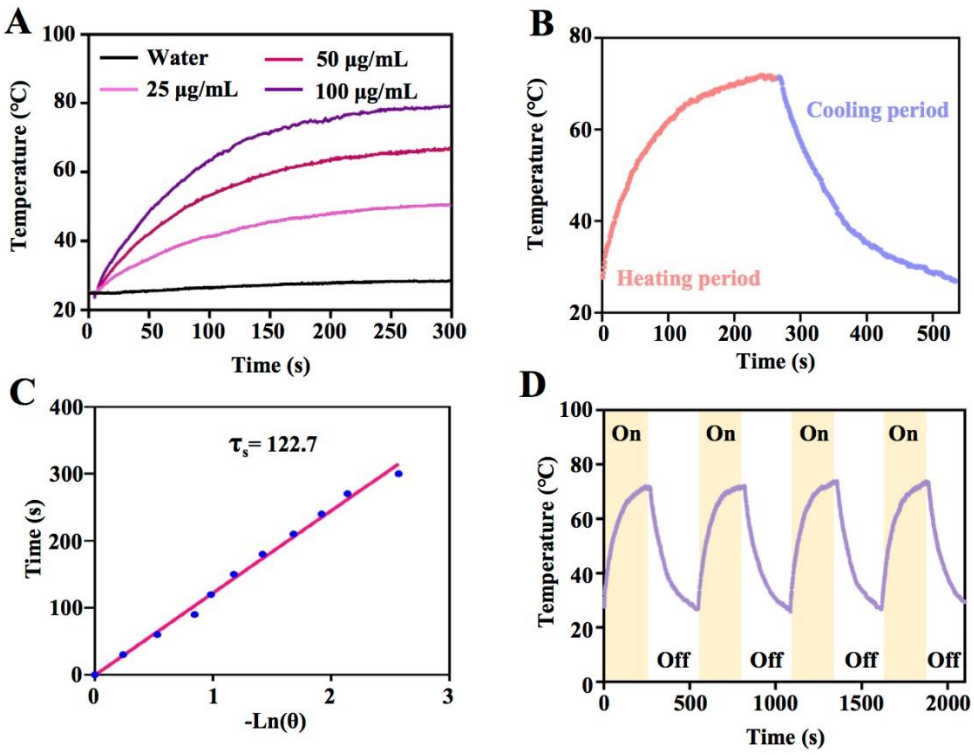

Figure S1. Photothermal properties of MXP.

(A) Temperature changes of MXP at various concentrations (0, 25, 50 and 100 μg/mL) after 808 nm NIR laser irradiation. (B) The temperature changes of MXP over laser irradiation on/off cycles at a constant concentration of 100 μg/mL under irradiation (1 W/cm^2, 5 min). (C) The heat transferring time constant was determined by using the linear time data from the cooling period versus the negative natural logarithm of the driving force temperature, which was obtained from the cooling stage. (D) The MXP solution was irradiated with an 808 nm continuous-wave laser (1 W/cm^2) for 300 s, and then cooled at room temperature for 300 s. We recorded 4 cycles continuously. Heating/cooling curves of MXP solution at a constant concentration of 100 μg/mL exposed to 808 nm NIR laser irradiation (1 W/cm^2) for four laser switched on/off cycles.

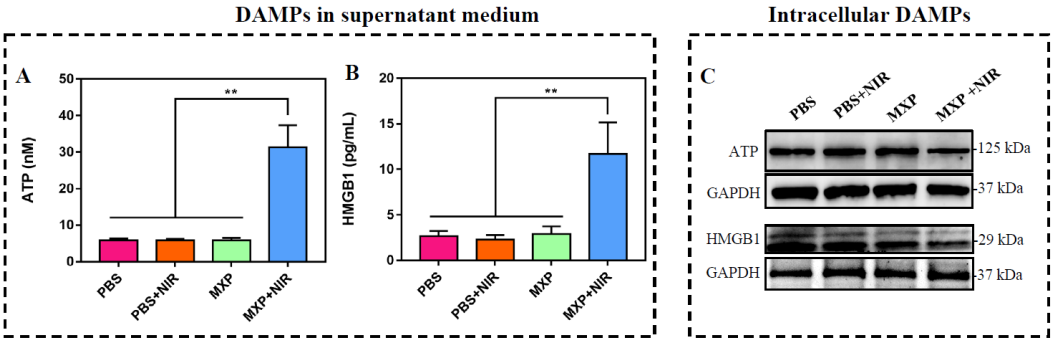

Figure S2. Detection of immunogenic cell death markers. (A) Concentrations of ATP in supernatant medium after different treatments. The data are represented as the means ± s.d. (n = 3). (B) ELISA results of HMGB1 concentrations in supernatant medium after different treatments. The data are represented as the means ± s.d. (n = 3). (C) Western blot results of intracellular DAMPs (ATP and HMGB1) in different treatment groups. For statistical significance, $^{**}P < 0.01$.

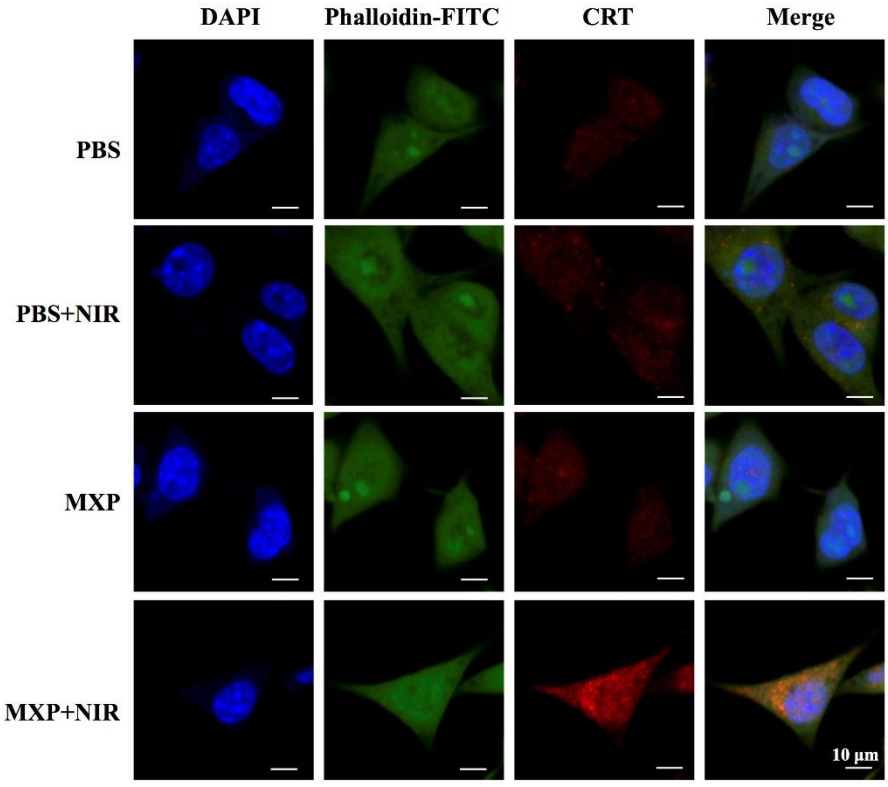

Figure S3. Detection of immunogenic cell death markers (CRT). Immunofluorescence staining of calreticulin (Red) in B16-OVA tumor cells. The cells were co-stained with DAPI (blue) and Phalloidin-FITC (green). Scale bar: 10 μm.

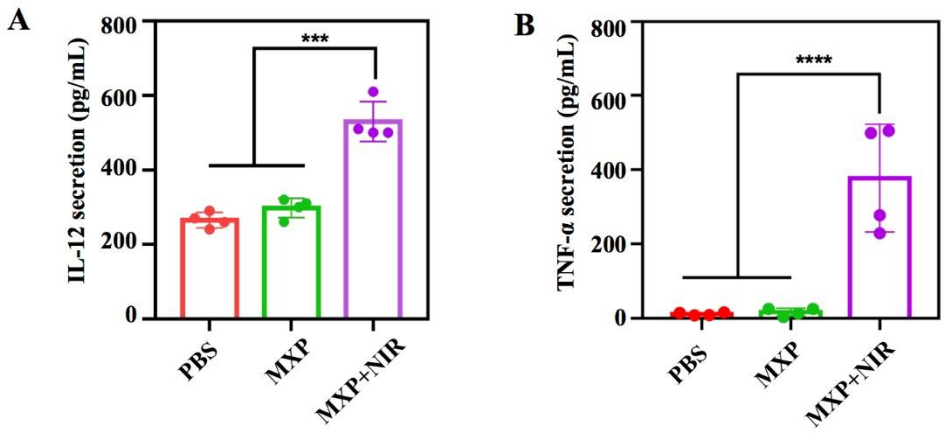

Figure S4. Cytokines secreted in the culture medium by DCs. Cytokines (A) IL-12 and (B) TNF-α secreted in the culture medium in transwell experiments *in vitro*. Significant differences are shown as follows: ****P*< 0.001 and *****P*< 0.0001.

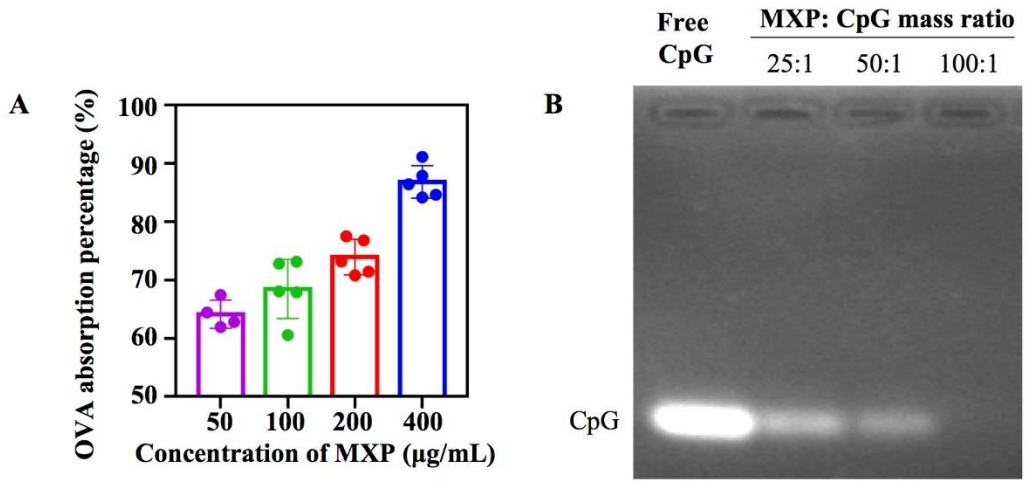

Figure S5. Carrier performance of MXP. (A) Model antigen OVA adsorption isotherms of MXP with varying initial concentrations. (B) Agarose gel electrophoresis of free CpG in the incubation supernatant at various MXP:CpG mass ratios.

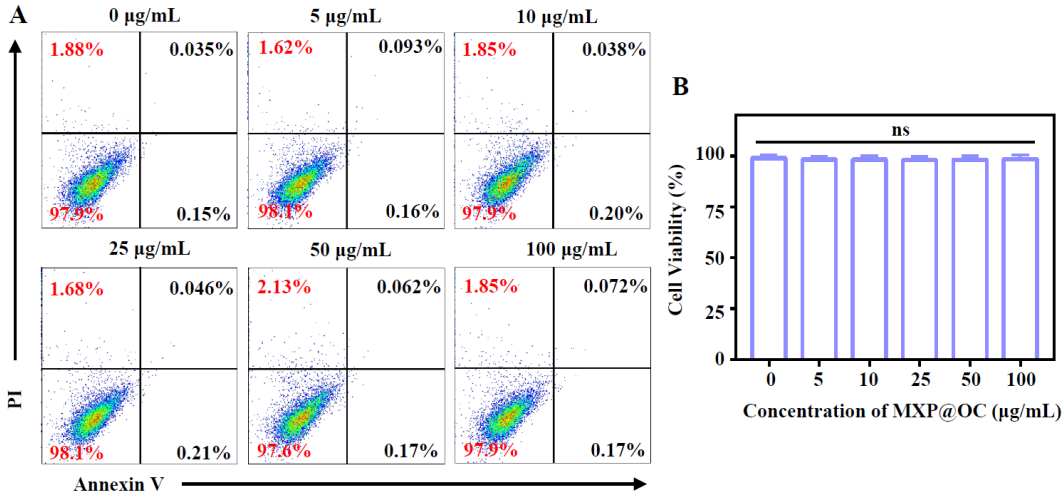

Figure S6. Cytotoxicity assay of mutuDCs cultured with MXP@OC at different concentrations. Data are presented as the means ± s.d. (n = 3).

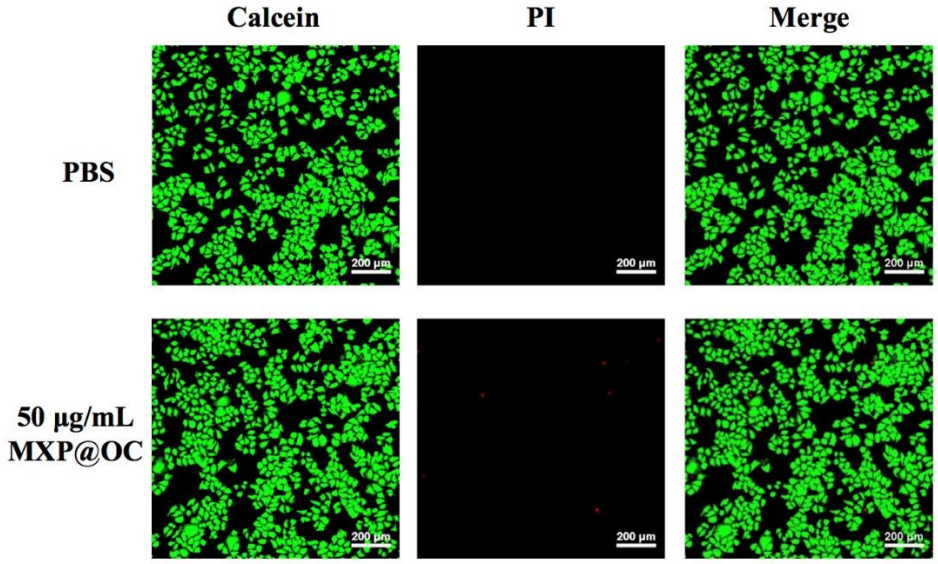

Figure S7. CLSM images of Calcein-AM/PI-stained DC2.4 cells treated with PBS and MXP@OC.

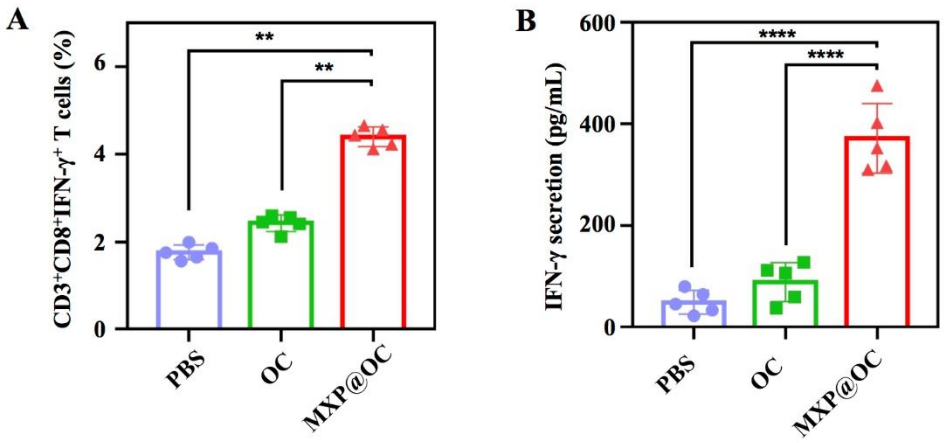

Figure S8. Detection of induced cytotoxic T-cell immune responses. (A) Flow cytometry analysis illustrating the proportion of $CD3^{+}CD8^{+}IFN\text{-}\gamma^{+}$ T cells and (B) IFN-γ secretion among splenocytes from tumor-bearing mice after restimulation with SIINFEKL *ex vivo*.

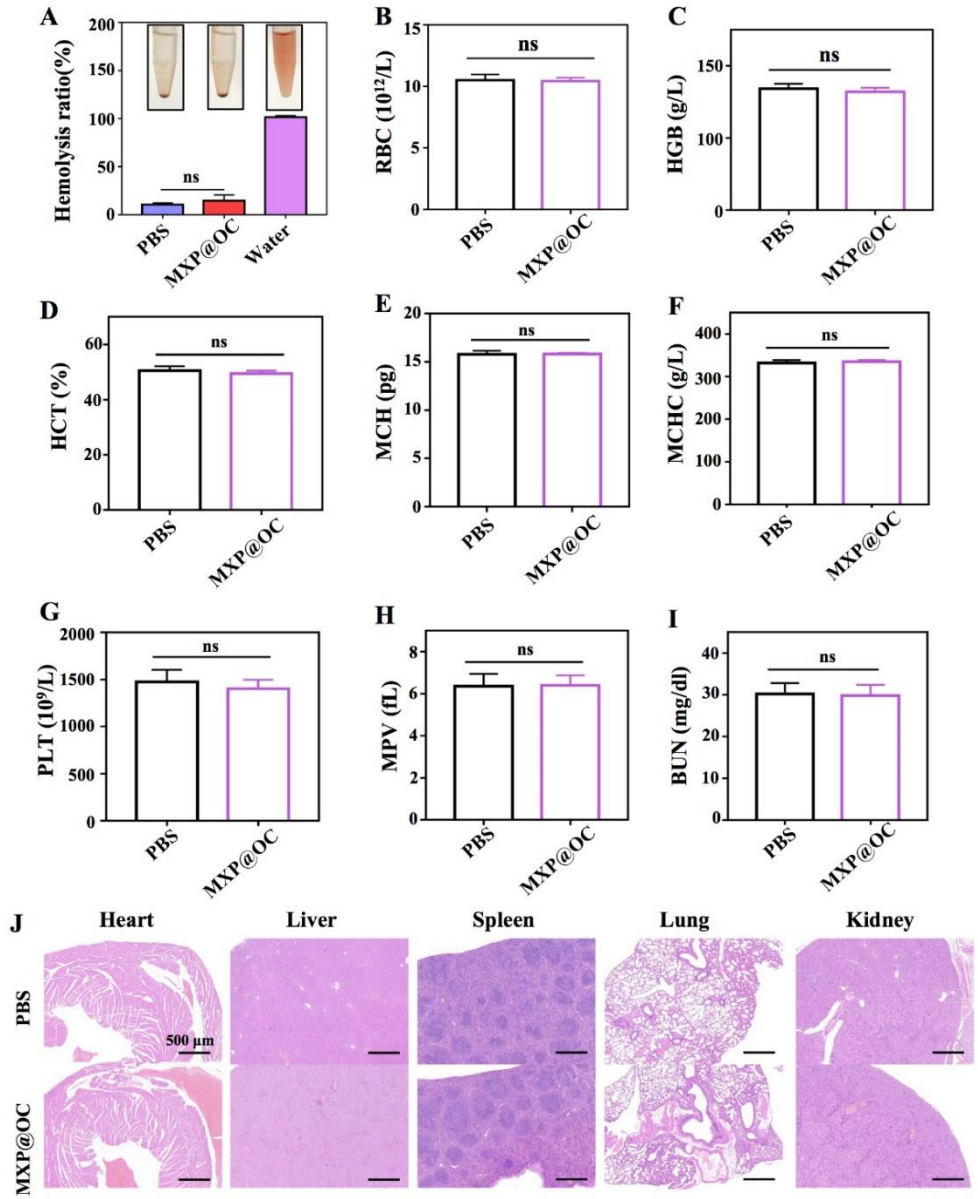

Figure S9. Biocompatibility of MXP@OC *in vivo*

(A) Representative pictures and hemolysis ratio of mouse erythrocytes incubated with 200 μg/mL MXP@OC for 2 h. (B) Number of red blood cells (RBC), (C) hemoglobin (HGB), (D) hematocrit (HCT), (E) mean corpuscular hemoglobin (MCH) levels, (F) mean corpuscular hemoglobin concentration (MCHC), (G) platelets (PLT), (H) mean platelet volume (MPV), and (I) blood urea nitrogen (BUN) in the blood at 28 days post-injection of PBS or MXP@OC. (J) H&E-stained sections of major organs (heart, liver, spleen, lung, and kidney) from mice immunized with PBS or MXP@OC. All data are presented as the means ± SD (n=5). ns, not significant.

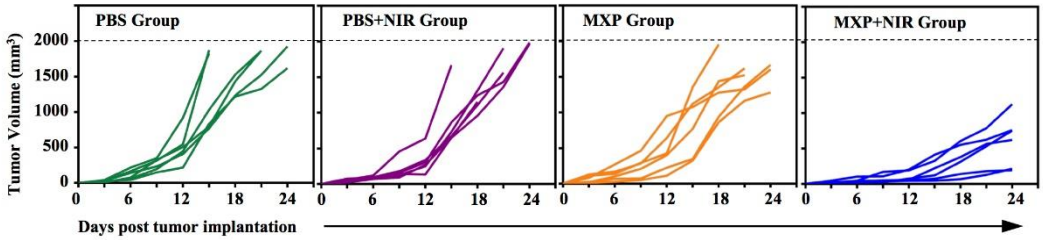

Figure S10. *In vivo* antitumor experiments of MXP-mediated PTT. Tumor growth curves of individual mice in different groups (n = 6 independent mice per group).

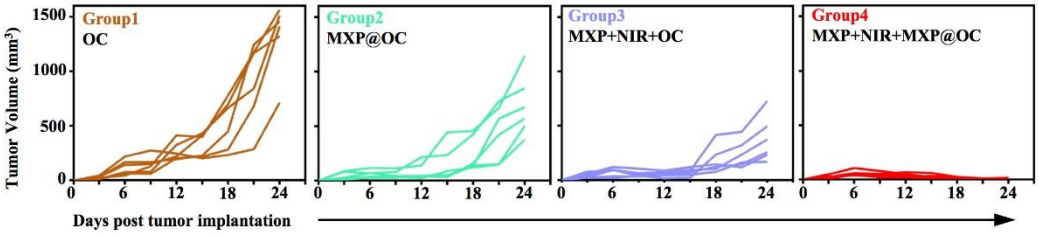

Figure S11. Combining MXP@OC nanovaccine with MXP-mediated PTT. Tumor growth curves for individual mice in different groups (n = 6 independent mice per group). (Group 1: OC; Group 2: MXP@OC; Group 3: MXP+NIR+OC; Group 4: MXP+NIR+ MXP@OC).